Quasiperiodic route to chaos in the Kerr-lens mode-locked Ti:sapphire laser

S. R. Bolton and M. R. Acton
Physics Department, Williams College, Williamstown, Massachusetts 01267
(Received 25 June 2000; published 3 November 2000)

We have performed an experimental study of the nonlinear dynamics in a Kerr-lens mode-locked Ti:sapphire laser producing ≈ 25 fs pulses. Grassberger-Procaccia and false nearest-neighbor analyses indicate that the pulse trains follow a quasiperiodic route to low-dimensional chaos. The experimental results agree quite well with a simulation based on the Gaussian four-by-four matrix formalism. Pulse-resolved measurements show that the instability in pulse energy is associated with instabilities in the pulse spectral and spatial profile.

PACS number(s): 42.65.Sf, 42.65.Re

I. INTRODUCTION

Femtosecond lasers are becoming increasingly important in science and technology. Fiber lasers hold great promise in optical communications, while high power solid state lasers now generate pulses of only a few optical cycles. Several distinct laser mechanisms have been discovered which generate <100 fs pulses, but all have in common the requirement of an optical nonlinearity to lock the phases of thousands of longitudinal modes. The nonlinearity which enables this mode locking, however, also makes short pulse lasers susceptible to a variety of dynamic instabilities, including chaos. Because nonlinearities are an inevitable part of any short-pulse system, it is important to understand the resulting dynamics in some detail. Furthermore, the nascent study of nonlinear dynamics in ultrafast lasers has revealed these lasers to be fruitful as model nonlinear systems.

Two of the most promising mode-locking mechanisms at present are coupled cavity and Kerr-lens mode locking (KLM). Coupled cavity configurations, such as additive pulse mode locking (APM) and the nonlinear optical loop mirror, are commonly used in short-pulse fiber lasers. APM is a passive mode-locking technique, in which a pair of optical cavities are precisely matched in length and coupled through a partial reflector. The main cavity contains the gain, while the control cavity contains a medium with an intensity-dependent refractive index—typically an optical fiber. A pulse traveling through the control cavity undergoes an intensity-dependent phase shift in the fiber, then returns to the partial reflector where it recombines interferometrically with the next pulse coming from the main cavity. This superposition creates a new, reshaped pulse, and can result in pulse shortening if the nonlinear phase in the control cavity is correct. APM lasers have produced pulses as short as 75 fs, using a variety of different gain media. There has been substantial recent work on the nonlinear dynamics of these ultrafast coupled cavity lasers. In picosecond Nd:YAG APM lasers period doubling, quasiperiodicity, and high-dimensional chaos have been both observed and modeled theoretically [1,2]. Observations of dynamic instabilities have also been made in fs NaCl:OH APM lasers [3–5]. In addition to period doubling, fs APM lasers display deterministic noise amplification, ''wiggly'' bifurcation phenomena, and a strong dependence of dynamics on cavity topology [4–6]. A number of common features are evident in the experiments and models of APM laser dynamics. First, the single mode optical fiber eliminates the possibility of transverse spatial dynamics, restricting instablilities to the temporal domain. Furthermore, the gain media in the APM lasers studied thus far (Nd:YAG and NaCl:OH) are strongly saturated by the passage of a single pulse. This gain saturation combines with the additive pulse mechanism to give significant temporal reshaping of the pulses. Theoretical work on the APM laser predicts that the pulses can have highly non-Gaussian, multi-peaked temporal profiles, which vary from pulse to pulse. Evidence for such pulse-reshaping has been found in the high dimensional dynamics of the Nd:YAG APM [1] which must originate in the degrees of freedom provided by changes in temporal pulse profile. Finally, the importance of group velocity dispersion (GVD) in coupled cavity optical systems has been clearly demonstrated, for both the case of passive ring resonators and active APM lasers. A very elegant demonstration of optical turbulence in a passive nonlinear fiber ring resonator driven by a series of ps pulses was performed by Steinmeyer *et al.* [7]. In this case the GVD of the system was the dominant variable controlling the degree of complexity.

Ultrafast lasers based on KLM are physically quite distinct from their APM counterparts. In KLM, the intensity-dependent index of refraction in the gain medium results in self-focusing of the fs pulses. This intensity-dependent, or Kerr, lens can be combined with either a physical aperture (hard aperturing) or with a spatially narrow gain profile (soft aperturing) to yield higher net gain for fs pulses than for cw light. The resulting energetic advantage for ultrashort pulses is combined with solitonic pulse shaping to give a very stable and flexible laser which produces pulses of <30 fs. GVD must be carefully managed in order to obtain short pulses from KLM lasers. Since the gain medium has significant positive GVD and self-phase modulation further chirps the pulses, an element with *negative* GVD is necessary in order to keep the pulses short and take advantage of solitonic pulse shaping. Such GVD compensation is typically provided by a prism pair (as shown in Fig. 1), which creates, via angular dispersion, a negative GVD proportional to the distance between the prisms. The prism glass itself has positive GVD; thus the total GVD provided by the prism pair can be controlled by varying the prism insertion. The total GVD is

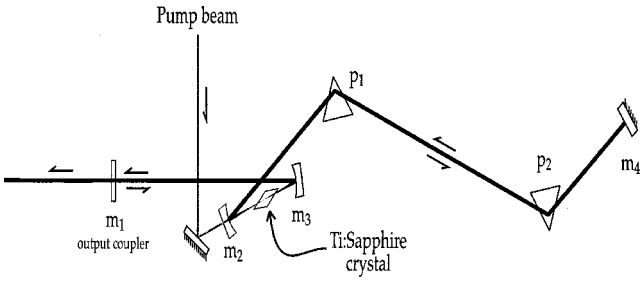

FIG. 1. Laser cavity schematic. M1 is a 12% output coupler, M2 and M3 are 10 cm radius of curvature high reflectors, and M4 is a flat high reflector. P1 and P2 are fused silica prisms.

most negative if the beam passes through just the tips of the prisms, and becomes less negative as the prism insertion is increased.

The gain medium most frequently used in KLM is Ti:sapphire, which has a gain spectrum centered at 800 nm and sufficient bandwidth to support a 3-fs pulse. The nonlinear dynamics of the KLM Ti:sapphire differ from that of the APM laser in several respects. First, the KLM mechanism couples the temporal and spatial evolution of pulses through the intensity-dependent lens, allowing the possibility of spatiotemporal dynamics. In addition, the KLM laser can support a small proportion of its energy lasing in higher order transverse modes. Spatiotemporal dynamics associated with coupling between multiple transverse modes has been observed by several groups, and can be associated with a transverse sweeping of the beam at tens of MHz [8,9]. Finally, Ti:sapphire has a very high saturation intensity, ≈ 100 kW/cm^2; thus the gain is not significantly saturatated by a single pulse. Thus, in the KLM Ti:sapphire, significant deviations of the pulse temporal profiles from Gaussian or $(\mathrm{sech})^2$ are not expected.

There have been several theoretical studies of dynamical instabilities in KLM Ti:sapphire lasers [10,11]. All of the studies predict chaotic dynamics, although the physical origins of the chaos differ. There have also been two recent experimental observations of instability in the pulse train of the Ti:sapphire laser [12,13]. A careful experimental characterization of the route to chaos in a KLM Ti:sapphire laser, however, has not previously been performed. In the present paper we provide such a characterization, including tests of the determinism of the observed instabilities and a demonstration that these indeed indicate low-dimensional spatiotemporal chaos.

II. EXPERIMENTAL SETUP

Experiments are performed on a KLM Ti:sapphire laser pumped by a frequency-doubled cw Nd:YVO_4 laser which produces 5.5 W at 514 nm. The cavity, shown in Fig. 1, is configured in an asymmetric ''X,'' with a 4.75-mm-gain crystal and 12% output coupler M1. The two 10-cm radius of curvature mirrors, M2 and M3, are 5.0 and 5.3 cm from the center of the gain crystal. The prism dispersion arm of the cavity, from M3 to M4, is 89.5 cm, while the distance from M2 to M1 is 61.5 cm. Two Brewster angle fused silica

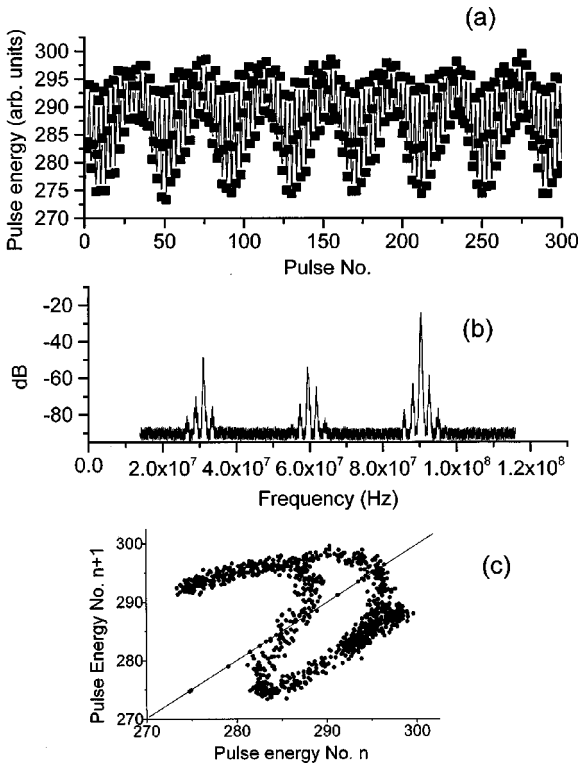

FIG. 2. Data measured in a quasiperiod-3 regime. (a) Pulse train, (b) rf spectrum, and (c) first return map (arbitrary units).

prisms are set 62 cm apart for dispersion compensation. The prism P2 is mounted on a computer-controlled translation stage to allow controlled insertion in 12.5-μm steps. The total length of the cavity is 166 cm, giving a pulse repetition rate of 90.3 MHz (a pulse separation of 11 ns). No hard aperture is used to mode lock the laser. A soft gain aperture is provided by the 20-μm pump spot in the Ti:sapphire crystal. In this configuration the laser is observed to mode lock extremely robustly. Bandwidth-limited pulses of approximately 25 fs are produced.

The laser exhibits a variety of dynamical regimes as the cavity parameters are varied. In order to characterize the dynamics, we measure the pulse train using an extremely low-noise InGaAs photodiode with 0.5 ns response. The photodiode is far too slow to resolve the temporal shape of the fs pulses—it simply gives the integrated energy of each pulse. Trains of 2000 pulses are acquired in single shot mode by a 4-GHz digital oscilloscope. The raw data are downloaded to a computer, where each pulse is fit by a fourth-order polynomial to give an accurate integrated pulse energy. Data obtained in this way have noise of less than 1%. Low-noise data are critical to a proper determination of chaotic dynamics, as many analysis algorithms are sensitive to noise contamination of otherwise deterministic data. Pulse trains from the same photodiode are simultaneously sent to an rf spectrum analyzer with 1-kHz resolution bandwidth.

III. PULSE TRAIN DYNAMICS

The laser dynamics depend on both pump power and prism insertion (net GVD). At low power and small prism

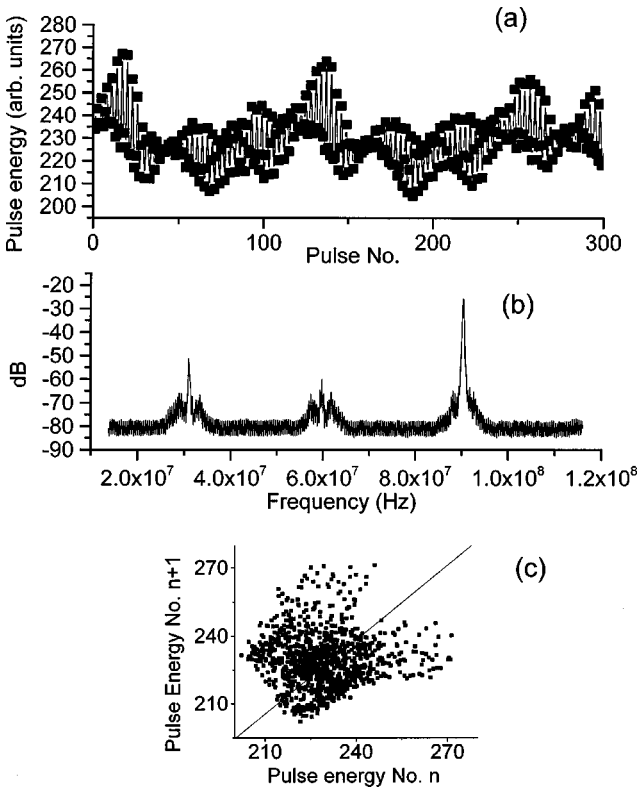

FIG. 3. Data measured in the chaotic regime. (a) Pulse train, (b) rf spectrum, and (c) first return map (arbitrary units).

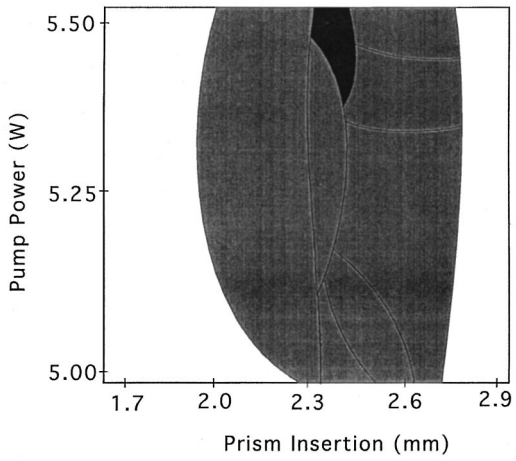

FIG. 4. Phase plot of period-1 (white), quasiperiodic (grey), and chaotic (black) regimes as a function of pump power and insertion of prism 2. Lines within quasiperiodic region indicate transitions between different modulation frequencies.

insertion, the laser operates in a stable, period-1 regime. As either prism insertion or pump power are increased, the pulse train becomes quasiperiodic, exhibiting very regular modulations of pulse energy over a time scale of 400–500 ns. One example of such a pulse train and the associated rf spectrum is shown in Figs. 2(a) and 2(b). Figure 2(c) shows the first return map of the data (a section through the phase space of the system). The closed loop indicates correlations of one pulse to the next, and shows that the trajectory in phase space moves on a torus. The precise depth and frequency of modulation vary among quasiperiodic regimes, depending on the prism insertion and pump power. As pump power and prism insertion are further increased, the quasiperiodic modulations suddenly snap into an aperiodic regime and the rf spectrum significantly broadens, indicating the possibility of chaos (Fig. 3). In this regime the first return map shows no discernable structure. Finally, as the prism insertion is further increased, the laser resumes quasiperiodic and ultimately period-1 oscillation. A summary of the pump power vs prism insertion phase diagram is shown in Fig. 4.

It should be noted that the data in Figs. 2 and 3 show both slow modulation (at 1.8 MHz in Fig. 2) and a much faster period-3 subharmonic at 30 MHz. It is the slow modulation which is characteristic of transitions through chaos. The period-3 subharmonic is due to coupling of multiple transverse modes, and is quite independent of the slow modulation. It is a common feature at high pump powers, where the aperture provided by the pump beam profile is not sufficient to suppress a small amount of lasing in higher-order transverse modes [8,9].

Although a broadened rf spectrum and aperiodic oscilloscope trace are necessary for chaos, they are not sufficient. Stochastic noise also has both of these features, and a careful analysis of the data is nesessary to determine whether deterministic chaos is, in fact, present. Our analysis starts with the reconstruction of a pseudo phase space from the one-dimensional time series data via the delay-coordinate technique [14]. The choice of delay coordinate is made using the linear and nonlinear correlation functions. We then use a combination of Grassberger-Procaccia analysis (GPA) and false nearest-neighbors (FNN) analysis to obtain the correlation and embedding dimensions for the data. These two analyses distinguish clearly between random noise (which is very high dimensional) and low-dimensional, deterministic chaos. In the GPA the correlation dimension D_2 is calculated as a function of the embedding dimension E. It is expected that, for low-dimensional chaotic data, $D_2(E)$ converges to D_2 of the underlying attractor, while for white noise D_2 increases linearly with unity slope. Figure 5(a) shows the results of a GPA of the aperiodic pulse train shown in Fig. 3. Here $D_2(E)$ clearly converges, indicating that the data are not merely white noise. However, the GPA is sensitive to linear as well as nonlinear correlations; thus a further check must be performed to ensure that colored noise is not responsible for the aperiodicity. It was pointed out in [15] that a comparison with so-called ''surrogate'' data, which have the same linear correlations as the measured data, can provide such a check. The surrogate data are produced by Fourier transforming the original data, randomizing the phases, and then reversing the Fourier transform. A comparison of the GPA analysis of the surrogate data with the original [Fig. 5(a)] clearly shows convergence in the experimental data which is absent in the surrogate. Thus we confirm that the data are indeed generated by a nonlinear, low dimensional, deterministic chaos. The embedding dimension of the attractor can be estimated using the FNN technique, in which the number of neighbors in an E-dimensional reconstructed phase space is compared with that in $E+1$ dimensions. For low-dimensional, deterministic chaos the number of false

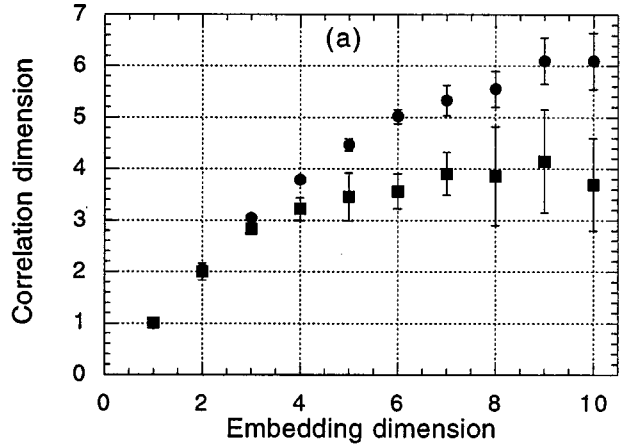

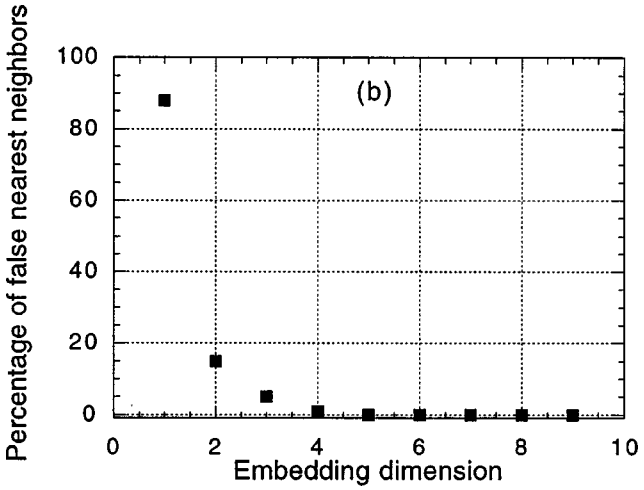

FIG. 5. Statistical analysis of chaotic data set shown in Fig. 3. (a) Grassberger-Procaccia analysis of true data (squares) and surrogate data (circles). (b) False nearest-neighbor analysis.

neighbors should fall rapidly to zero at a relatively small value of E. For high-dimensional chaos and for random noise the FNN will level off at a nonzero value, and may even rise again as E is increased. As shown in Fig. 5(b), the FNN analysis of our chaotic data set gives an embedding dimension of approximately 4.

Our analysis of the time series data indicates that the laser is undergoing a quasiperiodic route to low-dimensional chaos. To further understand the physics driving these dynamics, we study the optical spectrum and temporal autocorrelation of the pulses, using both time-averaged and pulse-resolved techniques, and compare these with the results of a simulation. These results are presented in the next two sections.

IV. TEMPORAL AND SPECTRAL MEASUREMENTS

Autocorrelations were performed to measure the changes in average pulsewidth as the laser moved from period 1, through quasiperiodicity and chaos. As shown in Fig. 6, these indicate a decrease in pulse width as the prism insertion is increased and the laser moves through quasiperiodicity,

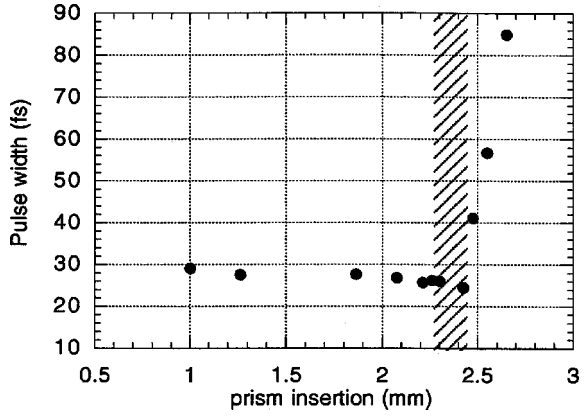

FIG. 6. Pulse width as measured from autocorrelation, as a function of the insertion of prism 2. Cross-hatched region corresponds to chaotic dynamics.

and a minimum pulse width in the chaotic regime. As the prism insertion is further increased and the chaos gives way to quasiperiodicity and then P1, the pulses lengthen rapidly. Further increasing the prism insertion causes the laser to stop mode locking.

The decrease in pulse width with increasing prism insertion can be understood from solitonic pulse shaping, in which the positive chirp generated by self-phase modulation is compensated by a negative chirp from negative GVD. Initially, as the prism insertion is increased, the net negative GVD of the cavity is decreased, and the total cavity GVD goes toward zero. The solitonic model gives for the pulse width τ_s of an ideal soliton

$$\tau_s = \frac{3.53|\mathcal{D}|}{\phi U}, \tag{1}$$

Here $|\mathcal{D}|$ is the GVD in fs^2 and ϕ gives the round trip phase shift per unit power (W^{-1}) in the Kerr medium [16]. In real lasers this expression becomes inaccurate as $|\mathcal{D}|$ goes to zero, as factors not included in the solitonic approximation become significant.

The evolution of the temporal pulse width shown in Fig. 6 is thus consistent with a crossing of the zero GVD point in or near the chaotic regime. Beyond this point, any further increase of the prism insertion brings the cavity into slightly positive total GVD, as observed in the rapid increase of the pulse width measured beyond the chaotic regime. For net positive GVD solitonic pulses are not possible, as the chirp induced by self-phase modulation is uncompensated for. Measurements of optical spectra are consistent with the autocorrelations, showing strong spectral broadening of the pulses as the prism insertion is increased, with a maximum spectral breadth of $\Delta\lambda \approx 60$ nm in the chaotic regime. As the prism insertion is further increased, the spectral width remains essentially unchanged, although the temporal width of the pulses increases. This is consistent with the increase in chirp expected in the regime of slightly positive net cavity GVD, and is confirmed by interferometric autocorreclations which show a strong, nonlinear chirp for the largest prism insertions.

Although the pulse shaping associated with net negative GVD and solitary pulses certainly gives the most stable operation of the KLM laser [16,17], it is also clear that, for sufficiently strong self-amplitude modulation provided by the Kerr lens, pulsing can continue to be energetically favorable through the zero GVD point [18]. Our data indicate that the laser undergoes a transition through chaos at high intracavity powers near zero GVD, when the pulses become very short. These circumstances combine to give high transient intensity, and thus strong nonlinearity due to self-phase modulation and self-focusing. Once the zero GVD point is crossed and the pulses start to lengthen again, the transient intensity rapidly drops. The self-phase modulation and self-focusing weaken, and the laser moves out of the chaotic regime [19].

V. SIMULATIONS

We compare our data with the results of a model based on the 4×4 matrix formalism for temporal and spatial propagation of Gaussian pulses [20,21]. The technique is similar to that used by Martinez and Chilla and by Hnilo and Marioni [10,22–24] for studies of the self-mode-locking and self-starting mechanisms in KLM lasers. Like the familiar *ABCD* matrices which describe spatial propagation of beams, the 4×4 formalism can handle up to quadratic variations in phase in the spatial and temporal evolution of the fields. The model has two important limitations. First, the formalism requires Gaussian beams. It cannot accurately represent either spatially non-Gaussian beams (such as those with higher-order transverse modes) or beams which are strongly reshaped in time (such as those observed in the APM laser). Second, the model cannot give a full description of self-phase modulation, since the approximation of the quadratic phase variation limits the formalism to linearly chirped beams. The self-phase modulation of a Gaussian beam, $I=e^{-\gamma t^2}$, yields a time-dependent frequency (chirp) of the form

$$\omega=\omega_0+\frac{2\pi n_2 L}{\lambda}\frac{\partial I(t)}{\partial t}=\omega_0+\frac{4\pi\gamma n_2 L}{\lambda}I_0 t e^{-\gamma t^2}. \quad (2)$$

Such a chirp is only linear near the peak of the pulse, where $t^2\ll 1/\gamma$. Despite these difficulties, the formalism we have adopted has a number of advantages. Most important, it allows for proper coupling of the temporal and spatial evolution of the pulses within a formalism simple enough to be numerically tractable. As discussed below, our experiments indicate that the approximation of Gaussian beams is appropriate for our experimental regime. We will not repeat the details of the matrix formalism here, as they are given in previous work [22,23]. The essentials of the model are as follows. The electric field of the pulse is described by

$$E(r,t)=E_0 e^{-ikr^2/2q}e^{-ikt^2/2p}, \quad (3)$$

where

$$\frac{1}{q}=\frac{\eta}{R}-\frac{i\eta\lambda}{\pi\sigma^2} \quad (4)$$

and

$$\frac{1}{p}=\frac{1}{k}\frac{\partial^2\phi}{\partial t^2}-\frac{i\eta\lambda}{\pi\tau^2} \quad (5)$$

describe the spatial and temporal complex beam parameters, repsectively. Here R is the phase-front radius of curvature, η the refractive index, λ the center wavelength, and k the center wave number of the pulse. U describes the pulse energy, τ the pulse width, σ the beam size, and $\partial^2\phi/\partial t^2$ the pulse chirp. Each optical element of the system can be written as a four-by-four matrix. In our case, each matrix separates into 2×2 diagonal blocks, as

$$M=\begin{bmatrix} A & B & 0 & 0 \\ C & D & 0 & 0 \\ 0 & 0 & K & I \\ 0 & 0 & J & L \end{bmatrix}. \quad (6)$$

The *ABCD* submatrix is precisely that found in the spatial matrix formalism for Gaussian beams. Propagation of the pulse through an optical element is achieved via the relationships between input and output pulse parameters,

$$q_{out}=\frac{Aq_{in}+B}{Cq_{in}+D}, \quad (7)$$

$$p_{out}=\frac{Kp_{in}+I/\lambda}{\lambda Jp_{in}+L}. \quad (8)$$

The *ABCD* submatrix takes care of the focusing mirrors and free space propagation. In the Ti:sapphire crystal both temporal and spatial reshaping must be considered, and we make several approximations to speed the computation. First, we neglect astigmatism and treat all elements as radially symmetric. In addition, beam size variations within the crystal are taken into account by using, in the matrices for self-phase modulation and self-focusing, an effective interaction length z equal to the confocal parameter of the beam. With these approximations, the Gaussian gain profile gives an imaginary part of C,

$$\mathrm{Im}(C)=\frac{-2\lambda}{\pi\sigma_p^2}\left(\frac{g}{1+g}\right), \quad (9)$$

where σ_p is the pump beam size in the crystal, and g is the (saturated) gain coefficient. Self-focusing in the rod gives the real part of C,

$$\mathrm{Re}(C)=-\frac{4n_2 Uz}{\tau\sigma^4}\left(\frac{2}{\pi}\right)^{3/2}, \quad (10)$$

and self-phase modulation (SPM) gives a temporal propagation coefficient

$$J=\frac{4n_2Uz}{\lambda\tau^3\sigma^2}\left(\frac{2}{\pi}\right)^{3/2}. \tag{11}$$

GVD (found in both the gain crystal and the double pass through the prism dispersion line) gives a temporal coefficient $I=2\pi\mathcal{D}$. Here $\mathcal{D}$ gives the magnitude of the GVD, $\mathcal{D}=\partial^2\phi/\partial\omega^2$. Finally, although no explicit bandwidth filter is placed in the cavity, it is appropriate to include some bandwidth limitation in the model to reflect the finite bandwidths of the gain and reflective optics. Treating these as a single Gaussian element colocated with the gain medium and having transmission profile $T(\omega)=e^{-\alpha\omega^2/2}$, we obtain an imaginary part of I given by $I=i2\pi\alpha$.

The procedure used in making the calculations is as follows. For each optical element the appropriate 4×4 matrix is created. A pulse with a particular q and p is seeded at the mirror M3, and propagated one round trip through the prism dispersion line. Before entering the gain medium the pulse parameters are recalculated and used to compute the values of the SPM and self-focusing matrix elements. The pulse is then propagated through the gain crystal and the nondipsersive end of the cavity. This procedure is repeated for 2000 iterations, with the pulse spatial and temporal parameters explicitly recalculated before each pass through the crystal. At each round trip the pulse energy, temporal and spatial widths, and chirp are saved as simulated time series data, to be compared with the experimental results. The simulation typically converges after less than 50 iterations. The parameters used in our calculation were $n_2=1.4\times10^{16}$ cm^2/W, $\alpha=20$ fs^2, and $\mathcal{D}=550$ fs^2 per pass for the gain crystal. Pulses were seeded with $U=100$ nJ, $\tau=50$ fs, $\sigma=1$ mm, and zero chirp. Both prism GVD and gain were varied to explore the dynamics of the system.

Results of the simulations are in good qualitative agreement with the experiment, showing a transition from stable, period-1 oscillation, through a series of quasiperiodic regimes, and finally to a chaotic regime, as total cavity GVD becomes less negative. Figure 7 shows one example of a quasiperiodic pulse train and the first return map of the train, from the simulation at a pump power of 5 W and a prism GVD of -1700 fs^2. Figure 8 shows the data from a chaotic regime, where the pump power is 5.5 W and the prism GVD is -1200 fs^2. The simulations give quasiperiodic modulation frequencies of the same order of magnitude ($\approx1-10$ MHz) as those seen in experiment, and these frequencies depend on pump power and GVD as observed experimentally.

As in the experiment, the simulations show a decrease in average pulse width as the laser moves toward chaos with decreasing negative GVD and a minimum average pulse width in the chaotic regime near $\mathcal{D}=0$. The quasiperiodic oscillations break into chaos when the pulses start to approach the bandwidth limit α. For 5.5 W pump power, the chaotic regime persists over a range of about $|\mathcal{D}|<100$ fs^2. When $\mathcal{D}>100$ fs^2, the laser returns to quasiperiodic oscillations with significantly longer pulses, as seen in the experiment.

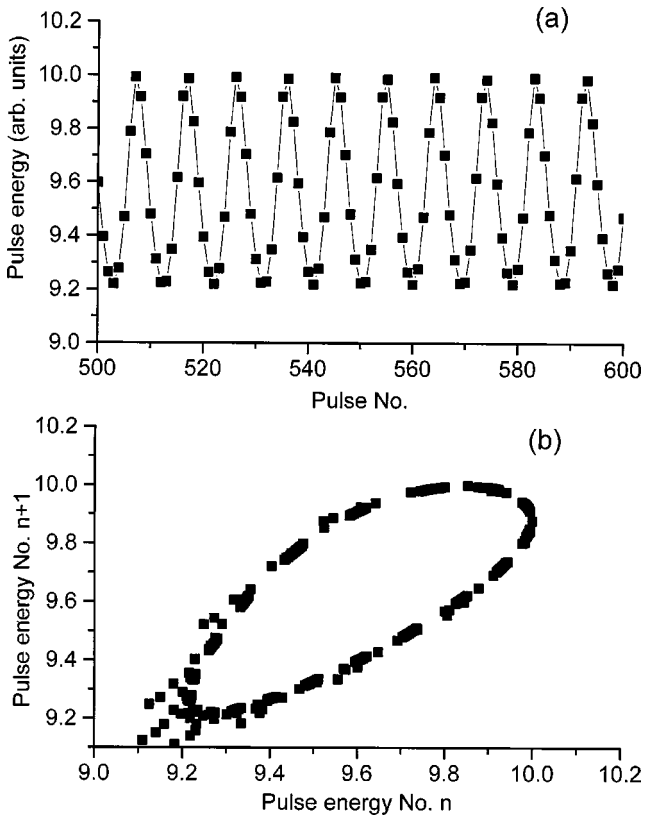

FIG. 7. Data from simulations, taken with pump power of 5 W and prism dispersion of -1700 fs^2. (a) Pulse train and (b) first return map (arbitrary units).

Not every aspect of the experimental data can be reproduced by the simulations. The experiments showed several regimes in which period three modulations were present in addition to slow quasiperiodicity. Period-3 modulations were not present in the simulations. However, previous work [8,9] has shown that very small amplitudes of higher-order spatial modes can give rise to these subharmonic oscillations. Such non-Gaussian modes are clearly not accounted for by the theory. However, throughout the transition to chaos a nearly Gaussian beam profile is measured experimentally. Thus, no more than a few percent of the energy could be in the higher order transverse modes, and the Gaussian approximation of the simulations is quite good. The temporal shaping of the pulses is also only approximately represented within our model. In a KLM Ti:sapphire laser, the most important pulse-width limiting factors near zero GVD are the finite gain and mirror bandwidths and third order dispersion [16,17]. Although under many circumstances it is the third-order dispersion which provides the strongest limits to pulse shortening [16,17,25], this effect cannot be included in our current model. Instead, we model the pulse-width limitation by a spectral bandwidth filter located at the position of the gain crystal. This certainly cannot reproduce the details of the spectral and phase profiles of the pulse, but does well in reproducing the overall dynamical regimes.

The final question to be addressed concerns the presence of temporal and spectral instabilities which may be associ-

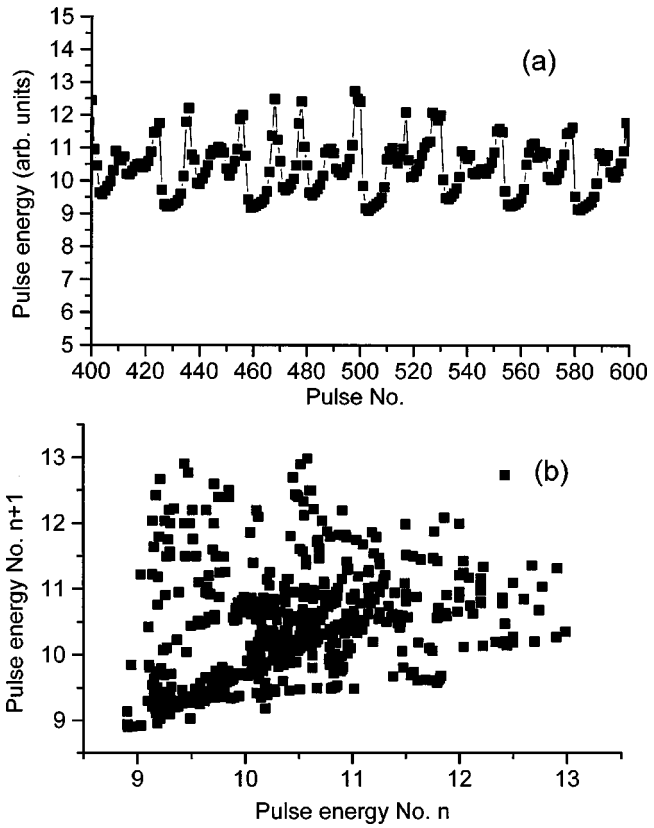

FIG. 8. Data from simulations in chaotic regime, taken with pump power of 5.5 W and prism dispersion of -1200 fs^2. (a) Pulse train and (b) first return map (arbitrary units).

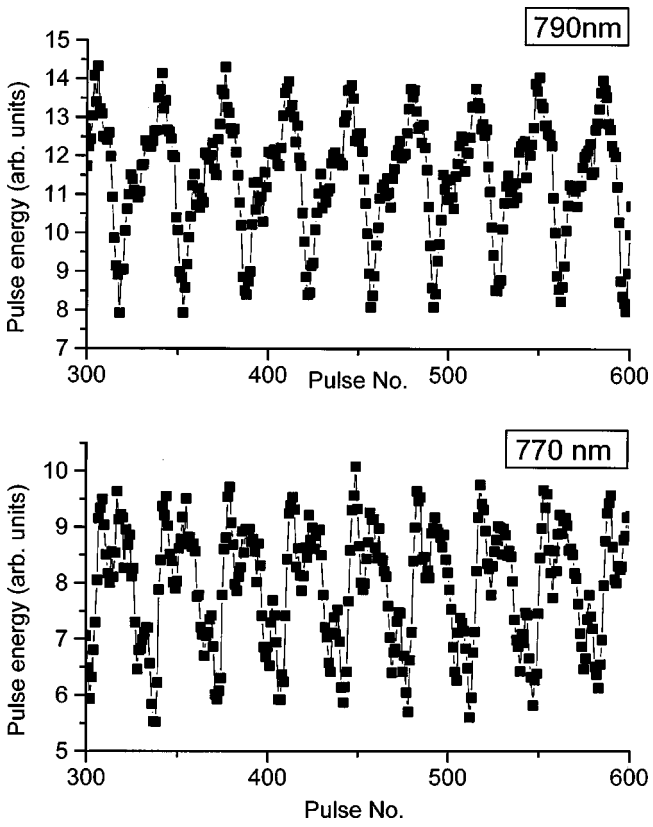

FIG. 9. Pulse trains measured over a 1-nm bandwidth in the quasiperiodic regime. (a) Centered at 790 nm and (b) centered at 770 nm.

ated with the energy instability presented here. Several groups have developed pulse resolved techniques for examining the variations in spatial and temporal profile which may occur between pulses in a nonperiod-1 pulse train [9,13]. The details of such an analysis are quite lengthy and beyond the scope of the work presented here; however, we will give a brief discussion of the general trends in our results. By measuring the pulse train on a small-area photodiode placed in the wing of the beam profile, we observe significant spatial modulations of the beam size in the quasiperiodic and chaotic regimes. This is in agreement with the theoretical work of Kalashnikov *et al.* [11] and also with the experiments of Kovalski *et al.* performed in a laser producing somewhat longer pulses [13]. In contrast with the work of Kovalski *et al.*, we also observe spectral variations between pulses. Spectral measurements were performed using a 0.55-m single-grating monochrometer to select a 1-nm slice of the beam spectral profile and project it onto a silicon photodiode with 1 ns response. The resulting pulse trains were analyzed using the digital oscilloscope and rf spectrum analyzer. An example of spectrally resolved pulse trains measured in a quasiperiodic regime is shown in Fig. 9. The amplitude of intensity modulations clearly varies with wavelength, indicating that different pulses within the quasiperiodic regime possess different spectral profiles, and thus likely also have different temporal profiles. Kovalski *et al.* [13] predicted that the increasing strength of SPM with decreasing pulse width would cause temporal reshaping to become important for pulses in the sub-50-fs regime, and our results are consistent with this prediction.

VI. CONCLUSIONS

We have observed a quasiperiodic route to low-dimensional chaos in a Kerr-lens mode-locked Ti:sapphire laser producing $\approx$25-fs pulses. The transition to chaos takes place near the point of zero GVD, at which the laser produces its shortest pulses. Although previous work had noted that KLM lasers tend to be unstable near zero GVD [16], the nature of the instability as low-dimensional chaos was not previously recognized. Nonlinear analysis of the experimental chaotic pulse trains indicates that the embedding dimension is approximately 4. The experimental results agree quite well with a simulation assuming pulses which are Gaussian in both space and time. Pulse-resolved measurements show that the instability in the pulse energy is associated with instabilities in both the temporal and spatial profiles of the pulses.

ACKNOWLEDGMENTS

This work was supported by the NSF under Grants No. ECS-9805888 and No. PHY-9724246, and by a Cottrell College Science Award from the Research Corporation.

[1] U. Morgner, L. Rolefs, and F. Mitschke, Europhys. Lett. **39**, 497 (1997).
[2] U. Morgner, L. Rolefs, and F. Mitschke, Opt. Lett. **21**, 1265 (1996).
[3] G. Sucha, S.R. Bolton, S. Weiss, and D.S. Chemla, Opt. Lett. **20**, 1794 (1995).
[4] G. Sucha, D.S. Chemla, and S.R. Bolton, J. Opt. Soc. Am. B **12**, 2487 (1998).
[5] E.J. Mozdy and C.R. Pollock, Phys. Lett. A **249**, 218 (1998).
[6] U. Morgner and F. Mitschke, Phys. Rev. A **55**, 3124 (1997).
[7] G. Steinmeyer, A. Schwache, and F. Mitschke, Phys. Rev. E **53**, 5399 (1996).
[8] D. Cote and H.M. van Driel, Opt. Lett. **23**, 715 (1998).
[9] S.R. Bolton, R.A. Jenks, C.N. Elkinton, and G. Sucha, J. Opt. Soc. Am. B **16**, 339 (1999).
[10] A. Hnilo, J. Opt. Soc. Am. B **12**, 718 (1995).
[11] V.L. Kalashnikov, I.G. Poloyko, V.P. Mikhailov, and D. von der Linde, J. Opt. Soc. Am. B **14**, 2691 (1997).
[12] Q. Xing, L. Chai, W. Zhang, and C. Wang, Opt. Commun. **162**, 71 (1999).
[13] M. Kovalski, A. Hnilo, and C. Gonzalez Inchauspe, Opt. Lett. **24**, 1638 (1999).
[14] H.D.I. Abarbanel, R. Brown, J.J. Sidorowich, and L.Sh. Tsimring, Rev. Mod. Phys. **65**, 1331 (1993).
[15] J. Theiler, B. Galdrikian, A. Longtin, S. Eubank, and J.D. Farmer, in *Nonlinear Modeling and Forecasting*, edited by M. Casdagli and S. Eubank, SFI Studies in the Sciences of Complexity Vol. XII (Addison-Wesley, Reading, MA, 1992), pp. 163–188.
[16] C. Spielmann, P.F. Curley, T. Brabec, and F. Krausz, IEEE J. Quantum Electron. **30**, 1100 (1994).
[17] T. Brabec, Ch. Spielmann, and F. Krausz, Opt. Lett. **17**, 748 (1992).
[18] D. Spence, P.N. Kean, and W. Sibbett, Opt. Lett. **16**, 42 (1991).
[19] From a practical point of view, Ti:sapphire lasers are typically adjusted to produce the shortest possible pulses consistent with a stable pulse train. Thus the lasers are generally operated with slightly negative net GVD and at intracavity powers low enough to avoid the onset of quasiperiodicity.
[20] A.G. Kostenbauder, IEEE J. Quantum Electron. **26**, 1148 (1990).
[21] S. Dijaili, A. Dienes, and J.S. Smith, IEEE J. Quantum Electron. **26**, 1158 (1990).
[22] O. Martinez and J. Chilla, Opt. Lett. **17**, 1210 (1992).
[23] J.L.A. Chilla and O.E. Martinez, J. Opt. Soc. Am. B **10**, 638 (1993).
[24] M. Marioni and A. Hnilo, Opt. Commun. **147**, 89 (1998).
[25] M.T. Asaki, C.P. Haung, D. Garvey, J. Zhou, H.C. Kapteyn, M.M. Murnane, Opt. Lett. **18**, 977 (1993).